

CERN-EP-2025-298
23 December 2025

Dihadron Transverse-Spin Asymmetries in Muon-Deuteron Deep-Inelastic Scattering

Abstract

In 2022, the COMPASS collaboration performed semi-inclusive measurements of deep-inelastic muon-scattering on a transversely polarised deuteron (^6LiD) target. From these data, transverse-spin-dependent dihadron asymmetries are extracted using pairs of oppositely charged hadrons. These asymmetries are directly sensitive to the quark transversity distributions and provide an independent handle on these fundamental quantities with respect to the Collins asymmetries measured in single-hadron production. The present results significantly improve upon the previous COMPASS deuteron measurements, which were the only available deuteron data worldwide, and reach a statistical precision comparable to that of the existing proton results from COMPASS. A small but nonzero asymmetry is observed at large Bjorken- x , consistent with theoretical expectations. A point-by-point extraction of the valence-quark transversity distributions yields, in particular, a substantially improved determination of the d -quark transversity. These measurements represent a major step towards a complete flavour mapping of the transverse-spin structure of the nucleon.

The COMPASS Collaboration

(to be submitted to Phys. Rev. Letters)

The COMPASS Collaboration

G. D. Alexeev²⁸, M. G. Alexeev^{20,19}, C. Alice^{20,19}, A. Amoroso^{20,19}, V. Andrieux³³,
V. Anosov²⁸, S. Asatryan¹, K. Augsten⁴, W. Augustyniak²³, C. D. R. Azevedo²⁶, B. Badelek²⁵,
R. Beck⁸, J. Beckers¹², Y. Bedfer⁶, V. Benesova⁵, J. Bernhard³⁰, F. Bradamante¹⁷,
A. Bressan^{18,17,*}, W.-C. Chang³¹, C. Chatterjee^{17,a}, M. Chiosso^{20,19}, S.-U. Chung^{12,k,k1},
A. Cicuttin^{17,16}, M. L. Crespo^{17,16}, D. D'Ago^{18,17}, S. Dalla Torre¹⁷, S. S. Dasgupta¹⁴,
S. Dasgupta^{17,f}, M. Dehpour⁵, F. Delcarro^{20,19}, I. Denisenko²⁸, O. Yu. Denisov¹⁹,
S. V. Donskov^{1,29}, N. Doshita²², Ch. Dreisbach¹², W. Dünneberger^{b,b1}, R. R. Dusaev^{1,29},
D. Ecker¹², P. Faccioli²⁷, M. Faessler^{b,b1}, M. Finger^{5,†}, M. Finger jr.⁵, H. Fischer¹⁰,
K. J. Flöthner⁸, W. Florian^{17,16}, J. M. Friedrich¹², V. Frolov²⁸, L.G. Garcia Ordóñez^{17,16},
O. P. Gavrichtchouk²⁸, S. Gerassimov^{29,12}, J. Giarra¹¹, D. Giordano^{20,19,h,h1}, A. Grasso^{20,19},
A. Gridin²⁸, M. Grosse Perdekamp³³, B. Grube¹², M. Grüner⁸, A. Guskov²⁸, P. Haas¹²,
D. von Harrach¹¹, M. Hoffmann^{8,a}, A. Hognmrtysyan¹, N. d'Hose^{6,a}, C.-Y. Hsieh³¹,
S. Ishimoto^{22,j}, A. Ivanov²⁸, T. Iwata²², V. Jary⁴, E. Jelinkova⁴, R. Joosten⁸, E. Kabu^{11,a},
F. Kaspar¹², A. Kerbizi^{18,17,*}, B. Ketzer⁸, G. V. Khaustov²⁹, T. Klasek⁵,
J. H. Koivuniemi^{7,33}, V. N. Kolosov^{1,29}, K. Kondo Horikawa²², I. Konorov^{29,12},
A. Yu. Korzenev²⁸, A. M. Kotzinian¹, O. M. Kouznetsov²⁸, A. Koval²³, F. Kunne⁶, K. Kurek²³,
R. P. Kurjata²⁴, A. Kveton⁵, K. Lavickova⁴, S. Levorato^{17,m}, Y.-S. Lian³¹, J. Lichtenstadt^{15,a},
P.-J. Lin³², R. Longo^{33,d}, V. E. Lyubovitskij²⁹, A. Maggiora¹⁹, N. Makke¹⁷,
G. K. Mallot^{30,10}, A. Maltsev^{28,*}, A. Martin^{18,17}, H. Marukyan¹, J. Marzec²⁴, J. Matoušek⁵,
T. Matsuda²¹, C. Menezes Pires²⁷, F. Metzger⁸, W. Meyer^{7,c}, M. Mikhasenko¹³,
E. Mitrofanov²⁸, D. Miura²², Y. Miyachi²², R. Molina^{17,16}, A. Movsisian¹, A. Moretti^{18,17},
A. Nagaytsev²⁸, D. Neyret⁶, M. Niemiec²⁵, J. Nový⁴, W.-D. Nowak^{11,n}, G. Nukazuka²²,
A. G. Olshevsky²⁸, M. Ostrick^{11,g,g1}, D. Panziera^{19,*}, B. Parsamyan^{1,19,30}, S. Paul¹²,
H. Pekeler⁸, J.-C. Peng³³, M. Pešek⁵, D. V. Peshekhonov²⁸, M. Pešková⁵, S. Platchkov⁶,
J. Pochodzalla¹¹, V. A. Polyakov^{28,29}, P. Pucci⁵, C. Quintans^{27,23}, G. Reicherz⁷, C. Riedl³³,
D. I. Ryabchikov^{29,12}, A. Rychter²⁴, A. Rymbekova²⁸, V. D. Samoylenko^{1,29,a}, A. Sandacz²³,
S. Sarkar^{14,†}, I. A. Savin²⁸, G. Sbrizzai¹⁷, H. Schmieden⁹, A. Selyunin²⁸, S. Serubun²⁸,
L. Sinha¹⁴, D. Spülbeck⁸, A. Srnka^{2,*}, M. Stolarski²³, M. Sulc^{3,i}, H. Suzuki²², S. Tessaro¹⁷,
F. Tessarotto¹⁷, A. Thiel⁸, F. Tosello^{19,1}, A. Townsend³³, V. Tskhay²⁹, B. Valinoti^{17,16},
B. M. Veit¹¹, J.F.C.A. Veloso²⁶, A. Vijayakumar³³, M. Virius⁴, M. Wagner^{8,e}, S. Wallner¹²,
K. Zaremba²⁴, M. Zavertyaev²⁹, M. Zemko⁴, E. Zemlyanichkina²⁸, M. Ziembicki²⁴

¹ A.I. Alikhanyan National Science Laboratory, 2 Alikhanyan Br. Street, 0036, Yerevan, Armenia^A

² Institute of Scientific Instruments of the CAS, 61264 Brno, Czech Republic^B

³ Technical University in Liberec, 46117 Liberec, Czech Republic^B

⁴ Czech Technical University in Prague, 16636 Prague, Czech Republic^B

⁵ Charles University, Faculty of Mathematics and Physics, 12116 Prague, Czech Republic^B

⁶ IRFU, CEA, Université Paris-Saclay, 91191 Gif-sur-Yvette, France

⁷ Universität Bochum, Institut für Experimentalphysik, 44780 Bochum, Germany^C

⁸ Universität Bonn, Helmholtz-Institut für Strahlen- und Kernphysik, 53115 Bonn, Germany^C

⁹ Universität Bonn, Physikalisches Institut, 53115 Bonn, Germany^C

¹⁰ Universität Freiburg, Physikalisches Institut, 79104 Freiburg, Germany^C

¹¹ Universität Mainz, Institut für Kernphysik, 55099 Mainz, Germany^C

¹² Technische Universität München, Physik Dept., 85748 Garching, Germany^C

¹³ Ludwig-Maximilians-Universität, 80539 München, Germany

¹⁴ Matrivani Institute of Experimental Research & Education, Calcutta-700 030, India^D

¹⁵ Tel Aviv University, School of Physics and Astronomy, 69978 Tel Aviv, Israel^E

¹⁶ Abdus Salam ICTP, 34151 Trieste, Italy

¹⁷ Trieste Section of INFN, 34127 Trieste, Italy

- 18 University of Trieste, Dept. of Physics, 34127 Trieste, Italy
 19 Torino Section of INFN, 10125 Torino, Italy
 20 University of Torino, Dept. of Physics, 10125 Torino, Italy
 21 University of Miyazaki, Miyazaki 889-2192, Japan^F
 22 Yamagata University, Yamagata 992-8510, Japan^F
 23 National Centre for Nuclear Research, 02-093 Warsaw, Poland^G
 24 Warsaw University of Technology, Institute of Radioelectronics, 00-665 Warsaw, Poland^G
 25 University of Warsaw, Faculty of Physics, 02-093 Warsaw, Poland^G
 26 University of Aveiro, I3N, Dept. of Physics, 3810-193 Aveiro, Portugal^H
 27 LIP, 1649-003 Lisbon, Portugal^H
 28 Affiliated with an international laboratory covered by a cooperation agreement with CERN
 29 Affiliated with an institute formerly covered by a cooperation agreement with CERN
 30 CERN, 1211 Geneva 23, Switzerland
 31 Academia Sinica, Institute of Physics, Taipei 11529, Taiwan^I
 32 Center for High Energy and High Field Physics and Dept. of Physics, National Central University, 300 Zhongda Rd., Zhongli 320317, Taiwan^I
 33 University of Illinois at Urbana-Champaign, Dept. of Physics, Urbana, IL 61801-3080, USA^J

* Corresponding author

^a Supported by the European Union's Horizon 2020 research and innovation programme under grant agreement STRONG-2020 - No 824093

^b Retired from Ludwig-Maximilians-Universität, 80539 München, Germany

^{b1} Supported by the DFG cluster of excellence 'Origin and Structure of the Universe' (www.universe-cluster.de) (Germany)

^c Also at ORIGINS Excellence Cluster, 85748 Garching, Germany

^d Also at Institut für Theoretische Physik, Universität Tübingen, 72076 Tübingen, Germany

^e Supported by the Max Planck Institute for Physics, 85748 Garching, Germany

^f Present address: NISER, Centre for Medical and Radiation Physics, Bhubaneswar, India

^g Also at University of Eastern Piedmont, 15100 Alessandria, Italy

^{g1} Supported by the Funds for Research 2019-22 of the University of Eastern Piedmont

^h Also at INFN TIFPA, 38123 Trento, Italy

^{h1} Also at Università di Trento, 38123 Trento, Italy

ⁱ Also at Chubu University, Kasugai, Aichi 487-8501, Japan

^j Also at KEK, 1-1 Oho, Tsukuba, Ibaraki 305-0801, Japan

^k Also at Dept. of Physics, Pusan National University, Busan 609-735, Republic of Korea

^{k1} Also at Physics Dept., Brookhaven National Laboratory, Upton, NY 11973, USA

^l Also at Fairmont State University, Department of Natural Sciences, 1201 Locust Ave, Fairmont, West Virginia 26554, USA

^m Also at Dept. of Physics, National Kaohsiung Normal University, Kaohsiung County 824, Taiwan

ⁿ Also at RIKEN Nishina Center for Accelerator-Based Science, Wako, Saitama 351-0198, Japan

[†] Deceased

^A Supported by the Higher Education and Science Committee of the Republic of Armenia (Armenia), within the framework of Scientific Project No 21AG-1C028

^B Supported by MEYS, Grants LM2023040, LM2018104, LTT17018 and GAUK60121, CZ.02.01.01/00/22_008/0004632 "FORTE", co-funded by the EU and Charles University Grant PRIMUS/22/SCI/017 (Czech Republic)

^C Supported by BMBF - Bundesministerium für Bildung und Forschung (Germany)

^D Supported by B. Sen fund (India)

^E Supported by the Israel Academy of Sciences and Humanities (Israel)

^F Supported by MEXT and JSPS, Grants 18002006, 20540299, 18540281 and 26247032, the Daiko and Yamada Foundations (Japan)

^G Supported by NCN, Grant 2020/37/B/ST2/01547 (Poland)

^H Supported by FCT, Grants DOI 10.54499/CERN/FIS-PAR/0022/2019 and DOI 10.54499/CERN/FIS-PAR/0016/2021 (Portugal)

^I Supported by the Ministry of Science and Technology (Taiwan)

^J Supported by the National Science Foundation, Grant no. PHY-1506416 (USA)

1 Introduction

In quantum chromodynamics (QCD), a fast-moving nucleon (proton or neutron) is a composite, dynamic system of quarks and gluons (partons) exhibiting both longitudinal and transverse motion. The collinear parton distribution functions (PDFs) describe the longitudinal momentum fraction x carried by partons inside the nucleon [1, 2] and form the cornerstone of QCD phenomenology, providing the foundation for global analyses and precision predictions in high-energy processes. The transverse-momentum-dependent (TMD) PDFs extend this framework by incorporating the partonic transverse momentum \mathbf{k}_T , thereby offering access to the three-dimensional momentum structure of the nucleon [3–5].

At leading twist, the full quark spin and momentum structure is described by eight TMD PDFs for each quark flavour, encompassing all possible correlations between quark spin, transverse momentum, and nucleon spin. Among them, the spin-averaged $f_1(x, \mathbf{k}_T^2)$, the helicity $g_1(x, \mathbf{k}_T^2)$, and the transversity $h_1(x, \mathbf{k}_T^2)$ distributions have collinear counterparts: upon integration over \mathbf{k}_T , they reduce to $f_1(x)$, $g_1(x)$, and $h_1(x)$. The remaining five TMDs vanish upon \mathbf{k}_T -integration.

The collinear transversity distribution $h_1(x)$ describe transversely polarized quarks inside a transversely polarized nucleon [2, 6–9]. It represents the difference in the probability for finding a quark with spin aligned versus anti-aligned with respect to the transverse spin of the nucleon. It is directly related to the nucleon tensor charge, currently being evaluated in lattice QCD [10, 11]. Being a chiral-odd function, h_1 can be measured only through its coupling to another chiral-odd partner. This property distinguishes it from chiral-even f_1 and g_1 and prevents its determination in inclusive deep-inelastic scattering (DIS).

At variance, the TMD transversity distribution $h_1(x, \mathbf{k}_T^2)$ can be accessed in single hadron production in semi-inclusive DIS (SIDIS) with transversely polarized targets through its convolution with the chiral-odd Collins fragmentation function H_1^\perp [12]. In the Drell–Yan process it couples with another transversity distribution or with the chiral-odd Boer–Mulders TMD PDF [13, 14]. In TMD factorization framework the observable asymmetries involve convolutions in transverse momentum. As a consequence, the determination of the TMD PDFs and FFs requires assumptions or parametrizations of their transverse-momentum shapes [2, 15]. Alternatively, one can employ various weighting techniques to access transverse momentum moments of the PDFs and FFs [16–20].

In practice, SIDIS measurements [21–26] offer significantly higher statistical precision than Drell–Yan data [27, 28] and enable a more direct flavour decomposition through the combined use of proton and deuteron (or neutron) targets and charge-separated hadron samples. For this reason, most of the present knowledge on the transversity distribution h_1 comes from global analyses that combine SIDIS and e^+e^- data, the latter providing essential information on the chiral-odd fragmentation functions (FFs) required for the extraction.

Despite the fact that the collinear transversity PDF $h_1(x)$ cannot be accessed in inclusive DIS, it can be measured in semi-inclusive production of oppositely charged hadron-pairs, where it couples to the polarized dihadron interference fragmentation function H_1^\lessgtr [29–31]. This approach is particularly important and unique because it allows for a direct extraction of $h_1(x)$ without requiring transverse-momentum-dependent factorization, thereby avoiding complications related to transverse-momentum convolutions and soft-factor effects. The same dihadron framework also applies to polarized proton-proton collisions, providing an independent access to $h_1(x)$ [32].

The dihadron fragmentation function H_1^\lessgtr , which couples to transversity in collinear factorization, can originate from different mechanisms. One arises from the interference between quantum amplitudes associated with two competing channels for hadron-pair production, such as the direct production of the pair versus its production through a resonance decay [29, 33], or the production of the pair from the decays of two different resonances [30]. Another mechanism is provided by the string- 3P_0 model, in which the string connecting, e.g. the scattered quark and the target remnant in a DIS event, breaks via the tunneling

of quark–antiquark pairs with correlated spins and transverse momenta in the relative 3P_0 state [34, 35]. As in the case of the Collins FF, the H_1^\leftarrow has been extracted in global analyses combining e^+e^- annihilation data from the Belle Collaboration [36] with SIDIS data, where it is determined simultaneously with the transversity distribution [37–39].

The dihadron TSAs have been measured to be nonzero by HERMES [40] and by COMPASS [41–43] on transversely polarised proton targets. For flavour separation, measurements with neutron or deuteron targets are required. Prior to this work, the only such result was the COMPASS measurement with a transversely polarised deuteron target from the 2002–2004 data set [41], where the asymmetries were found to be compatible with zero within uncertainties.

This work presents new COMPASS results on dihadron TSAs, extracted from the 2022 data set collected with a transversely polarised deuteron target. It constitutes a natural continuation of the single-hadron transverse spin asymmetry analysis recently published in Ref. [26], now extended to the dihadron channel.

2 Formalism

The coordinate frame for dihadron production in SIDIS and the definitions of the relevant angles are provided in Fig. 1. The relevant momenta are the incoming lepton momentum \mathbf{l} , the virtual-photon momentum \mathbf{q} , and the relative hadron momentum $\mathbf{R} = \xi_2 \mathbf{p}_1 - \xi_1 \mathbf{p}_2$, where \mathbf{p}_1 and \mathbf{p}_2 are the momenta of the two selected final-state hadrons, and $\xi_i = z_i / (z_1 + z_2)$ with z_1 and z_2 the fractions of the virtual-photon energy carried by hadron 1 (positive) and hadron 2 (negative), respectively. The azimuthal angle ϕ_S of the spin of the nucleon is defined between the lepton scattering plane (spanned by \mathbf{l} and \mathbf{l}') and the transverse-spin component \mathbf{S}_T , while ϕ_R denotes the angle between the lepton scattering plane and the plane containing \mathbf{q} and the transverse component of the relative momentum \mathbf{R}_T .

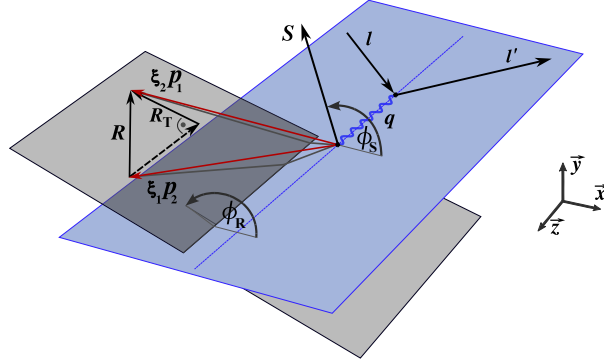


Fig. 1: Dihadron production coordinate frame and definition of the relevant vectors and azimuthal angles.

At leading twist and after integration over the total transverse momentum of the hadron pair, the differential cross section for dihadron production on a transversely polarized nucleon can then be written as [33, 41]

$$\frac{d^7\sigma}{d\cos\theta dM_{hh} d\phi_R dz dx dy d\phi_S} = \frac{\alpha^2}{2\pi Q^2 y} \times \left((1-y + \frac{y^2}{2}) F_{UU} + S_T (1-y) \sin\theta F_{UT}^{\sin\phi_{RS}} \sin\phi_{RS} \right). \quad (1)$$

Here, α is the fine-structure constant. The variable y denotes the fraction of the lepton energy (in the laboratory frame) transferred to the virtual photon, and Q^2 is the negative squared four-momentum transfer. The variables $z = z_1 + z_2$, M_{hh} , and θ correspond to the fraction of virtual-photon energy carried by the hadron pair, its invariant mass, and the polar angle of the positive hadron with respect to the two-hadron boost axis in the pair rest frame. Here, $\phi_{RS} = \phi_R - \phi_{S'} = \phi_R + \phi_S - \pi$, where $\phi_{S'}$ is the azimuthal angle of the spin vector of the fragmenting quark [22].

The structure function F_{UU} represents the spin-averaged contribution to the dihadron production cross section, corresponding to the case of an unpolarized beam and an unpolarized target. At leading twist, it is given by

$$F_{UU} = \sum_q e_q^2 f_1^q(x) D_{1,q}(z, M_{\text{hh}}^2, \cos\theta). \quad (2)$$

The sum runs over the quark and antiquark flavours q with charge e_q , and $D_{1,q}(z, M_{\text{hh}}^2, \cos\theta)$ denotes the unpolarized quark dihadron fragmentation function (FF).

The spin-dependent term $F_{UT}^{\sin\phi_{\text{RS}}}$ is proportional to the product of the transversity PDF $h_1^q(x)$ and the dihadron FF of transversely polarized quarks $H_{1,q}^{\leftarrow}(z, M_{\text{hh}}^2, \cos\theta)$:

$$F_{UT}^{\sin\phi_{\text{RS}}} = \frac{|\mathbf{p}_1 - \mathbf{p}_2|}{2M_{\text{hh}}} \sum_q e_q^2 h_1^q(x) H_{1,q}^{\leftarrow}(z, M_{\text{hh}}^2, \cos\theta) \quad (3)$$

The dihadron TSA $A_{UT}^{\sin\phi_{\text{RS}}}$ is given by the ratio of the two structure functions:

$$A_{UT}^{\sin\phi_{\text{RS}}} = \frac{|\mathbf{p}_1 - \mathbf{p}_2| \sum_q e_q^2 h_1^q(x) H_{1,q}^{\leftarrow}(z, M_{\text{hh}}^2, \cos\theta)}{2M_{\text{hh}} \sum_q e_q^2 f_1^q(x) D_{1,q}(z, M_{\text{hh}}^2, \cos\theta)}. \quad (4)$$

The dihadron TSA is extracted from the number of hadron pairs

$$N_{\text{hh}}(x, y, z, M_{\text{hh}}^2, \cos\theta, \phi_{\text{RS}}) \propto \sigma_{\text{UU}} (1 + f(x, y) P_{\text{T}} D_{\text{nn}}(y) \sin\theta A_{UT}^{\sin\phi_{\text{RS}}} \sin\phi_{\text{RS}}), \quad (5)$$

where $f(x, y)$ is the target-polarisation dilution factor accounting for the fraction of polarizable nucleons in the target material, P_{T} is the transverse target polarisation, and $D_{\text{nn}}(y)$ is the transverse-spin transfer coefficient.

3 Experimental Data and Event Selection

The present analysis closely follows the procedures established in previous COMPASS dihadron studies [41, 42], including event selection criteria, kinematic cuts, and the extraction method for azimuthal asymmetries. The data analyzed in this work are the same as those used for the Collins and Sivers asymmetry measurements reported in Ref. [26], where the experimental apparatus, data taking, and event selection are described. The data were collected by the COMPASS experiment [44] at CERN during the 2022 run, using a 160 GeV/ c naturally polarized μ^+ beam scattering off a transversely polarized deuteron (^6LiD) target. The experimental setup included a two-stage spectrometer equipped with tracking detectors, calorimetry, and particle identification systems to ensure precise reconstruction of the scattered muon and produced hadrons.

The analysis is based on events that fulfill deep-inelastic scattering conditions: $Q^2 > 1 \text{ (GeV}/c)^2$, $0.1 < y < 0.9$ and hadronic invariant mass $W > 5 \text{ GeV}/c^2$. For dihadron studies, at least two oppositely charged hadrons originating from the interaction vertex are required. These hadrons must have $z_{1,2} > 0.1$ and $z = z_1 + z_2 < 0.9$ to suppress exclusive contributions. The selection $M_{\text{hh}} > 0.3 \text{ GeV}/c^2$ is adopted to avoid the low-mass threshold region.

The target consisted of three cylindrical cells, 30, 60, and 30 cm in length and 1.5 cm in radius, which were polarised in alternating directions to minimise acceptance effects. The target polarization was reversed

in the middle of each of the ten data-taking periods of the 2022 run to minimize systematic effects. Data from the two polarization orientations were then combined to extract the transverse-spin asymmetries.

The TSAs are extracted by fitting the distribution of hadron-pair yields [Eq. (5)] as a function of ϕ_{RS} using an unbinned maximum-likelihood method. The extracted observable is $\langle A_{UT}^{\sin\phi_{RS}} \sin\theta \rangle$, integrated over θ (see Ref. [41]). In the COMPASS acceptance, θ peaks near $\pi/2$ with $\langle \sin\theta \rangle = 0.94$, and the $\cos\theta$ distribution is symmetric about zero. The fit function includes the $\sin\phi_{RS}$ modulation, and the extracted fitted amplitudes are normalized by $P_T f(x, y) D_{nn}(y)$. The average target polarization during the 2022 data-taking was approximately 0.50 with a relative uncertainty of about 3%, estimated from regular NMR calibrations. The dilution factor varies between 0.35 and 0.45 depending on kinematics. Its uncertainty is estimated to be 2%. Systematic uncertainties are assessed by varying the event selection criteria, testing alternative binning and fit ranges, and evaluating the stability of the results over the different data-taking periods. In addition, so-called false asymmetries are extracted by reassigning the target polarization orientation in cells and found to be consistent with zero within statistical uncertainties. All these studies confirm the robustness of the extraction method. Further details of the analysis technique can be found in Refs. [41, 42].

4 Results

The extracted dihadron TSAs are presented in Fig. 2 as a function x , z , and M_{hh} . The statistical uncertainties on the extracted asymmetries range from 0.5% to 2% depending on the kinematic bin, while the total point-to-point systematic uncertainties, shown by the gray bands, are below 60% of the statistical ones. The uncertainties are reduced by a factor of about 2-3 compared to the previous COMPASS deuteron measurement [41]. No significant signal is observed over the full kinematic range. The measured asymmetries remain small, typically below the percent level, and are statistically compatible with zero in most bins. This behavior is qualitatively consistent with expectations for a deuteron target, where cancellations between u - and d -quark contributions suppress the net asymmetry. A hint of a nonzero asymmetry is observed at large x , where the transversity distribution is expected to be sizable and the u -quark contribution dominates. No significant signal is observed in the ρ^0 resonance region.

The overall trend of the asymmetries agrees with the JAM (orange band) and MAP (purple band) global fit predictions [39, 45], which are based on e^+e^- , SIDIS, and pp two-hadron data TSA, including, in particular, previous COMPASS deuteron and proton results [41, 42]. The dihadron FFs and h_1^u and h_1^d are extracted simultaneously in the global QCD fits. The difference between the two models and the size of the shown statistical uncertainty bands is driven by the differences in the approaches, the data sets used, and various constraints and assumptions adopted by the groups.

In Fig. 2, the measured asymmetries are also compared with results from simulations of DIS events on a transversely polarized deuteron target using the string- 3P_0 model (green band) [35, 47]. In this approach, the color field between the scattered quark and the target remnant is modeled by a relativistic string. The breaking of the string into smaller segments describes the hadronization process. It occurs through tunneling of quark-antiquark pairs in the relative 3P_0 state, thus correlating the spin and transverse momentum of the quarks [34]. Such mechanism gives rise to a nonzero Collins FF and H_1^ζ if the fragmenting quark is transversely polarized [35]. The simulations were performed with the PYTHIA generator [48] using the StringSpinner package [46]. The latter enables spin effects via the string- 3P_0 model. The polarization of the fragmenting quark is parameterised using the point-by-point extractions of $h_1^{u\nu}(x)$ and $h_1^{d\nu}(x)$ obtained in Ref. [26]. As seen in the figure, the simulated asymmetries agree with the data within the uncertainties across all kinematic variables. The error bands reflect the statistical uncertainties of the parameterised transversity PDFs, while statistical uncertainties of the simulations are negligible.

The improvement in the knowledge of the transversity distributions achieved with the present measurement

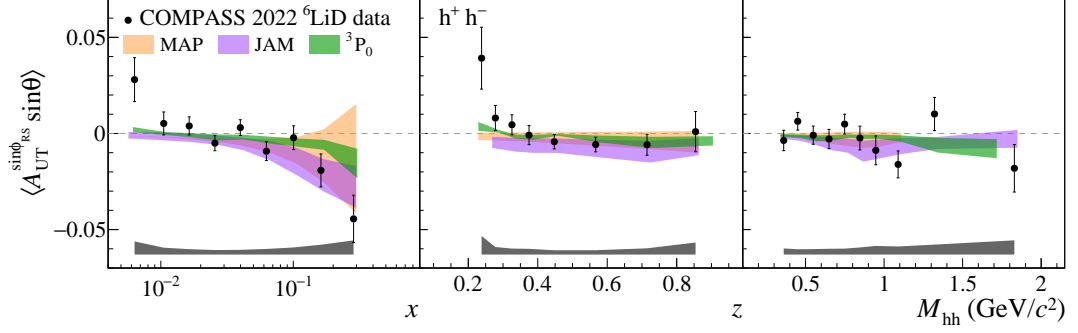


Fig. 2: Measured dihadron TSA as a function of x , z , and M_{hh} . The gray bands illustrate the associated systematic uncertainties. For comparison, the calculations from different models based on Refs. [45] (JAM), [39] (MAP) and [46] (3P_0) are also shown.

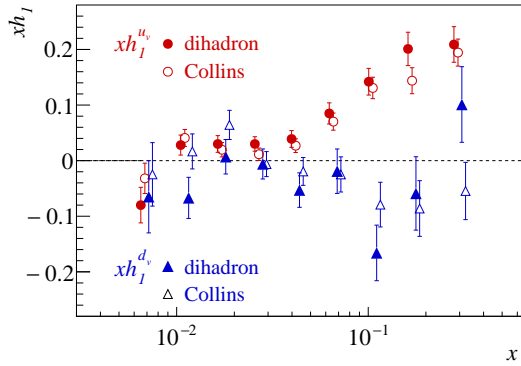


Fig. 3: The u_v (red circle) and d_v (blue triangles) valence-quark transversity in the different x bins, extracted from the full set of COMPASS measurements of the dihadron TSAs (closed points) and the Collins asymmetries (open points) [26]. Error bars represent statistical uncertainties.

has been evaluated by extracting, point by point, $h_1^{u_v}(x)$ and $h_1^{d_v}(x)$ from the dihadron TSAs, following the leading-order procedure of Ref. [49]. This extraction method requires neither parameterizations of transversity nor of the fragmentation functions, and it does not rely on Monte Carlo simulations. As in the case of the Collins asymmetries [26], the essential inputs are the measurements of the TSAs in SIDIS off proton and deuteron targets in the same kinematic range, and the corresponding asymmetries measured in e^+e^- annihilation.

Both $h_1^{u_v}$ and $h_1^{d_v}$ have been extracted from the dihadron TSAs using, first, only the previously published COMPASS results [41, 42] and, subsequently, the full data set including the present high-statistics deuteron measurement. With the complete set of COMPASS results, the statistical uncertainties are reduced by about a factor of two for both $h_1^{u_v}$ and $h_1^{d_v}$, clearly illustrating the impact of the new measurement. The results obtained using the full COMPASS data are shown in Fig. 3 as closed red circles and blue triangles. The u -quark transversity is well determined and clearly positive in the valence region, while $h_1^{d_v}$ is predominantly negative and lies within the Soffer bound [50], which is not imposed in the extraction. For comparison, the open points in Fig. 3 show the transversity values obtained from the point-by-point extraction [26] using the measured Collins asymmetries. The agreement between the valence transversities extracted from the Collins TSAs, based on transverse-momentum-dependent factorization of single-hadron production, and from the dihadron TSAs, based on collinear factorization of dihadron production, is quite good. This consistency supports the validity of both frameworks, in line with the conclusion drawn from the COMPASS study of the transverse-momentum-weighted Sivers asymmetries [20].

5 Conclusions

Transverse-spin-dependent dihadron asymmetries have been measured using the 2022 COMPASS data collected with a transversely polarised deuteron target. The statistical precision of the present results is comparable with that of the existing proton data and represents a substantial improvement over the previous measurement from the 2002–2004 deuteron data. This enables a more detailed investigation of the transverse spin structure of the nucleon within the collinear framework. The results show a non-zero trend at large x , consistent with expectations for the transversity distribution, while no significant signal is observed across the rest of the kinematic range. A comparison with recent theoretical predictions based on global fits reveals good agreement. The new data has an important potential to reduce the systematic and statistical uncertainties and constrain the parameterizations for the transversity PDFs. A bin-by-bin extraction of the transversity PDFs demonstrates that the deuteron data provide crucial sensitivity, especially to the d -quark transversity distribution, complementing existing measurements on proton targets and contributing to a more balanced flavour separation.

6 Acknowledgments

We gratefully acknowledge the support of the CERN management and staff and the skill and effort of the technicians of our collaborating institutes. We also thank JAM and MAP collaborations, in particular D. Pitonyak, C. Cocuzza and M. Radici for providing us with their calculations.

References

- [1] R. P. Feynman, *Photon–Hadron Interactions* (W. A. Benjamin, Reading, Massachusetts, 1972).
- [2] J. C. Collins, *Foundations of Perturbative QCD* (Cambridge University Press, 2011).
- [3] A. Kotzinian, *Nucl. Phys. B* **441**, 234 (1995), [arXiv:hep-ph/9412283](#) .
- [4] P. J. Mulders and R. D. Tangerman, *Nucl. Phys. B* **461**, 197 (1996), [Erratum: *Nucl.Phys.B* 484, 538–540 (1997)], [arXiv:hep-ph/9510301](#) .
- [5] A. Bacchetta, M. Diehl, K. Goeke, A. Metz, P. J. Mulders, and M. Schlegel, *JHEP* **02**, 093, [arXiv:hep-ph/0611265](#) .
- [6] J. P. Ralston and D. E. Soper, *Nucl. Phys. B* **152**, 109 (1979).
- [7] X. Artru and M. Mekhfi, *Z. Phys. C* **45**, 669 (1990).
- [8] R. L. Jaffe and X.-D. Ji, *Nucl. Phys. B* **375**, 527 (1992).
- [9] V. Barone, A. Drago, and P. G. Ratcliffe, *Phys. Rept.* **359**, 1 (2002), [arXiv:hep-ph/0104283](#) .
- [10] C. Alexandrou, K. Cichy, M. Constantinou, K. Jansen, A. Scapellato, and F. Steffens, *Phys. Rev. D* **98**, 091503 (2018), [arXiv:1807.00232 \[hep-lat\]](#) .
- [11] C. Alexandrou, S. Bacchio, J. Finkenrath, C. Iona, G. Koutsou, Y. Li, and G. Spanoudes, *Phys. Rev. D* **111**, 054505 (2025), [arXiv:2412.01535 \[hep-lat\]](#) .
- [12] J. C. Collins, *Nucl. Phys. B* **396**, 161 (1993).
- [13] D. Boer and P. J. Mulders, *Phys. Rev. D* **57**, 5780 (1998), [arXiv:hep-ph/9711485](#) .
- [14] S. Arnold, A. Metz, and M. Schlegel, *Phys. Rev. D* **79**, 034005 (2009), [arXiv:0809.2262 \[hep-ph\]](#) .
- [15] J. C. Collins, D. E. Soper, and G. Sterman, *Nucl. Phys. B* **194**, 445 (1982).

- [16] A. M. Kotzinian and P. J. Mulders, *Phys. Rev. D* **54**, 1229 (1996), [arXiv:hep-ph/9511420](#) .
- [17] A. M. Kotzinian and P. J. Mulders, *Phys. Lett. B* **406**, 373 (1997), [arXiv:hep-ph/9701330](#) .
- [18] D. Boer, L. Gamberg, B. Musch, and A. Prokudin, *JHEP* **10**, 021, [arXiv:1107.5294 \[hep-ph\]](#) .
- [19] M. Aghasyan, H. Avakian, E. De Sanctis, L. Gamberg, M. Mirazita, B. Musch, A. Prokudin, and P. Rossi, *JHEP* **03**, 039, [arXiv:1409.0487 \[hep-ph\]](#) .
- [20] M. G. Alexeev *et al.* (COMPASS), *Nucl. Phys. B* **940**, 34 (2019), [arXiv:1809.02936 \[hep-ex\]](#) .
- [21] A. Airapetian *et al.* (HERMES), *Phys. Rev. Lett.* **94**, 012002 (2005), [arXiv:hep-ex/0408013](#) .
- [22] E. S. Ageev *et al.* (COMPASS), *Nucl. Phys. B* **765**, 31 (2007), [arXiv:hep-ex/0610068](#) .
- [23] C. Adolph *et al.* (COMPASS), *Phys. Lett. B* **717**, 376 (2012), [arXiv:1205.5121 \[hep-ex\]](#) .
- [24] C. Adolph *et al.* (COMPASS), *Phys. Lett. B* **744**, 250 (2015), [arXiv:1408.4405 \[hep-ex\]](#) .
- [25] A. Airapetian *et al.* (HERMES), *JHEP* **12**, 010, [arXiv:2007.07755 \[hep-ex\]](#) .
- [26] G. D. Alexeev *et al.* (COMPASS), *Phys. Rev. Lett.* **133**, 101903 (2024), [arXiv:2401.00309 \[hep-ex\]](#) .
- [27] M. Aghasyan *et al.* (COMPASS), *Phys. Rev. Lett.* **119**, 112002 (2017), [arXiv:1704.00488 \[hep-ex\]](#) .
- [28] G. D. Alexeev *et al.* (COMPASS), *Phys. Rev. Lett.* **133**, 071902 (2024), [arXiv:2312.17379 \[hep-ex\]](#) .
- [29] J. C. Collins and G. A. Ladinsky, (1994), [arXiv:hep-ph/9411444](#) .
- [30] R. L. Jaffe, X.-m. Jin, and J. Tang, *Phys. Rev. Lett.* **80**, 1166 (1998), [arXiv:hep-ph/9709322](#) .
- [31] A. Bianconi, S. Boffi, R. Jakob, and M. Radici, *Phys. Rev. D* **62**, 034008 (2000), [arXiv:hep-ph/9907475](#) .
- [32] M. Radici, A. M. Ricci, A. Bacchetta, and A. Mukherjee, *Phys. Rev. D* **94**, 034012 (2016), [arXiv:1604.06585 \[hep-ph\]](#) .
- [33] A. Bacchetta and M. Radici, *Phys. Rev. D* **74**, 114007 (2006), [arXiv:hep-ph/0608037](#) .
- [34] X. Artru, in *Proc. of XIII Advanced Research Workshop on High Energy Spin Physics (DSPIN-09)* (Dubna, JINR., 2009) p. 33., [arXiv:1001.1061 \[hep-ph\]](#) .
- [35] A. Kerbizi, X. Artru, Z. Belghobsi, F. Bradamante, and A. Martin, *Phys. Rev. D* **97**, 074010 (2018), [arXiv:1802.00962 \[hep-ph\]](#) .
- [36] A. Vossen *et al.* (Belle), *Phys. Rev. Lett.* **107**, 072004 (2011), [arXiv:1104.2425 \[hep-ex\]](#) .
- [37] A. Courtoy, A. Bacchetta, M. Radici, and A. Bianconi, *Phys. Rev. D* **85**, 114023 (2012), [arXiv:1202.0323 \[hep-ph\]](#) .
- [38] M. Radici, A. Courtoy, A. Bacchetta, and M. Guagnelli, *JHEP* **05**, 123, [arXiv:1503.03495 \[hep-ph\]](#) .
- [39] M. Radici and A. Bacchetta, *Phys. Rev. Lett.* **120**, 192001 (2018), [arXiv:1802.05212 \[hep-ph\]](#) .
- [40] A. Airapetian *et al.* (HERMES), *JHEP* **06**, 017, [arXiv:0803.2367 \[hep-ex\]](#) .

- [41] C. Adolph *et al.* (COMPASS), *Phys. Lett. B* **713**, 10 (2012), [arXiv:1202.6150 \[hep-ex\]](#) .
- [42] C. Adolph *et al.* (COMPASS), *Phys. Lett. B* **736**, 124 (2014), [arXiv:1401.7873 \[hep-ex\]](#) .
- [43] G. D. Alexeev *et al.* (COMPASS), *Phys. Lett. B* **845**, 138155 (2023), [arXiv:2301.02013 \[hep-ex\]](#) .
- [44] P. Abbon *et al.* (COMPASS), *Nucl. Instrum. Meth. A* **577**, 455 (2007), [arXiv:hep-ex/0703049](#) .
- [45] C. Cocuzza, A. Metz, D. Pitonyak, A. Prokudin, N. Sato, and R. Seidl (Jefferson Lab Angular Momentum (JAM)), *Phys. Rev. D* **109**, 034024 (2024), [arXiv:2308.14857 \[hep-ph\]](#) .
- [46] A. Kerbizi and L. Lönnblad, *Comput. Phys. Commun.* **292**, 108886 (2023), [arXiv:2305.05058 \[hep-ph\]](#) .
- [47] A. Kerbizi, X. Artru, and A. Martin, *Phys. Rev. D* **104**, 114038 (2021), [arXiv:2109.06124 \[hep-ph\]](#) .
- [48] C. Bierlich *et al.*, *SciPost Phys. Codeb.* **2022**, 8 (2022), [arXiv:2203.11601 \[hep-ph\]](#) .
- [49] A. Martin, F. Bradamante, and V. Barone, *Phys. Rev. D* **91**, 014034 (2015), [arXiv:1412.5946 \[hep-ph\]](#) .
- [50] J. Soffer, *Phys. Rev. Lett.* **74**, 1292 (1995), [arXiv:hep-ph/9409254](#) .